# Microwave and Terahertz Surface Resistance of $MgB_2$ Thin Films

**B. B. Jin,[1] T. Dahm,[2] F. Kadlec,[3] P. Kuzel,[3] A. I. Gubin,[1] Eun-Mi Choi,[4] Hyun Jung Kim,[4] Sung-IK Lee,[4] W. N. Kang,[5] S. F. Wang,[6] Y. L. Zhou,[6] A. V. Pogrebnyakov,[7,8] J. M. Redwing,[8] X. X. Xi,[7,8] and N. Klein[1]**

The knowledge of the surface resistance $R_s$ of superconducting thin film at microwave and terahertz (THz) regions is significant to design, make and assess superconducting microwave and THz electronic devices. In this paper we reported the $R_s$ of $MgB_2$ films at microwave and THz measured with sapphire resonator technique and the time-domain THz spectroscopy, respectively. Some interesting results are revealed in the following: (1) A clear correlation is found between $R_s$ and normal-state resistivity right above $T_c$, $\rho_0$, i.e., $R_s$ decreases almost linearly with the decrease of $\rho_0$. (2) A low residual $R_s$, less than 50 $\mu\Omega$ at 18 GHz is achieved by different deposition techniques. In addition, between 10 and 14 K, $MgB_2$ has the lowest $R_s$ compared with two other superconductors $Nb_3Sn$ and the high-temperature superconductor $YBa_2Cu_3O_{7-\delta}$(YBCO). (3) From THz measurement it is found that the $R_s$ of $MgB_2$ up to around 1 THz is lower than that of copper and YBCO at the temperature below 25 K. (4) The frequency dependence of $R_s$ follows $\omega^n$, where $\omega$ is angular frequency, and $n$ is power index. However, n changes from 1.9 at microwave to 1.5 at THz. The above results clearly give the evidences that $MgB_2$ thin film, compared with other superconductors, is of advantage to make superconducting circuits working in the microwave and THz regions.

## 1. INTRODUCTION

The discovery of binary metallic $MgB_2$ with a superconducting transition $T_c$ of 39 K has stimulated great scientific interest and potential applications [1]. A number of experiments and calculations have demonstrated that the pairing symmetry is of conventional s-wave type, however, with two gaps of different size [2–7] Band structure calculations have shown that its Fermi surface consists of four bands: two $\sigma$-type two-dimensional cylindrical hole sheets (formed by B $p_{xy}$ orbits) and two $\pi$-type three-dimensional tubular networks, from the $\pi$ bonding and antibonding bands (formed by B $p_z$ orbits). This compound offers a realistic two-gap system for fundamental investigation.

As is commonly known, superconducting electronic devices made of low- and high-$T_c$

[1]Institut für Schichten und Grenzflächen (ISG) and cni, Center of Nanoelectronic Systems for Information Technology, Forschungszentrum Jülich, 52425 Jülich, Germany.

[2]Universität Tübingen, Institut für Theoretische Physik, Auf der Morgenstelle 14, 72076 Tübingen, Germany.

[3]Institute of Physics, Academy of Sciences of the Czech Rep., Na Slovance 2, 182 21 Praha 8, Czech Republic.

[4]National Creative Research Initiative Center for Superconductivity, Department of Physics, Pohang University of Science and Technology, Pohang 790-784, Korea.

[5]Department of Physics, Pukyung National University, Pusan 608-737, Korea.

[6]Laboratory of Optical Physics, Institute of Physics and Center of Condensed Matter Physics, Chinese Academy of Science, Beijing 100080, P. R. China.

[7]Department of Physics, The Pennsylvania State University, University Park 16802, Pennsylvania.

[8]Department of Material Science and Engineering, The Pennsylvania State University, University Park 16802, Pennsylvania.

superconductor have offered superior performance in the frequency range from microwave to terahertz (THz) [8–13]. $MgB_2$ is also expected to provide similar performance because of the relative high $T_c$, the s-wave pair symmetry and the relatively long coherence length [1,3,15,16]. The s-wave pair symmetry suggests that residual losses ought to be very low. Furthermore, $R_s$ is proportional to $\exp(-\Delta(0)/kT)$ for $T < T_c/2$, where $\Delta(0)$ is the size of energy gap at zero temperature. It means that $R_s$ of $MgB_2$ thin film may achieve low $R_s$ values at 20 K due to the relative high $T_c$. This temperature could easily be accessible with modern cryocoolers. This working temperature is impossible for other s-wave superconductors, e.g., Nb, NbN, and $Nb_3Sn$ because their $T_c$s are lower than 20 K. Another important property is the long coherence length $\xi_0$, which is around 50 nm. Microwave application will also benefit from this long coherence length because grain boundaries will not play an important role in the microwave nonlinearity. The intrinsic nonlinear response will be much easier to achieve in $MgB_2$ thin film, which may yield a large power handling. Moreover, long $\xi_0$ is crucial for the fabrication of $MgB_2$ Josephson junction. The success of the junction will give great opportunities for $MgB_2$ in the millimeter and THz detectors, which usually have the performance unattainable by the semiconductor devices.

Much effort, so far, has been devoted to the investigation of the microwave and THz properties of $MgB_2$ thin films [17,18–26] The measurements on residual surface resistance $R_{res}$, however, indicate large values [18–21]. Also, intermodulation measurement points to the model of Josephson coupled gains [23]. This means that extrinsic properties, to some extent, have a large influence on microwave properties. In addition, there is an increased demand to know the electromagnetic response in the THz region for designing THz devices and estimating the performance because the design and estimation are usually numerical simulations, which strongly rely on the input of precisely measured material properties of $MgB_2$ at THz frequencies as well as on theoretical models. In this paper we will firstly present microwave surface resistance measurements on eight $MgB_2$ thin films with the sapphire resonator technique. A correlation between $R_s$ and material parameter is observed. Then, we discuss the temperature dependence of $R_s$ at low temperature for random orientation, c-axis orientation and epitaxial thin films, and conclud that grain boundary may not have a large influence on $R_s$.

The comparison of $R_s$ is carried out between $MgB_2$ and $Nb_3Sn$ and the high-temperature superconductor $YBa_2Cu_3O_{7-\delta}$(YBCO). We also report measurement on an epitaxial thin film with time-domain THz spectroscopy (TDTS) [27, 28]. The results show that $R_s$ of $MgB_2$ is lower than that of copper at 1THz below $T_c$. Finally, combining the $R_s$ value at microwave and THz, the frequency dependence following $\omega^n$ is observed, However, $n$ changes from 1.9 at microwave region to around 1.5 at THz region, where $\omega$ is angular frequency and $n$ is power index.

## 2. SAMPLES

Eight $MgB_2$ thin films of different quality are prepared by chemical vapor deposition (CVD) with post-deposition annealing [29], pulsed laser ablation (PLD) with in situ annealing [30] and in situ hybrid physical–chemical vapor deposition (HPCVD) [31] methods, respectively. The three films deposited on MgO substrates by the CVD method are randomly oriented with a thickness of about 600 nm. The three films deposited on $Al_2O_3$ by PLD are c-axis oriented with a thickness of about 400 nm. The remaining two films are epitaxial films deposited by HPCVD on $Al_2O_3$ and SiC, respectively, with the thickness of about 100 nm (on $Al_2O_3$) and 300 nm (on SiC), respectively. $T_c$ measurements show that all samples exhibit a sharp transition of the dc resistivity with a width of less than 0.3 K. For the sample on SiC, the highest $T_c$ of 41.3 K was observed.

## 3. MICROWAVE MEASUREMENTS

In our previous work a sapphire resonator technique has been successfully employed to measure $Z_s = R_s + j\omega\mu_0\lambda$ of $MgB_2$ thin films at a frequency $f = \omega/2\pi = 18$ GHz [17,32,33] Here $\omega$ is the angular frequency, $\mu_0$ is the free-space permeability, and $\lambda$ is the penetration depth. The same method is used in our present investigation. We found in the measurements that the residual surface resistance $R_{res}$ ($R_{res} = R_s(T \to 0)$) of the $MgB_2$ thin film is less than the resolution for $R_s$ of our setup (about 50 $\mu\Omega$). Hence, the measured $R_s(T)$ actually represents the change of $R_s$.

Figure 1a showed $R_s$ at 15 and 20 K dependence on normal-state resistivity $\rho_0$ at temperature just above $T_c$. A nearly linear decrease of $R_s$ was easily found with the decrease of $\rho_0$. In the study of
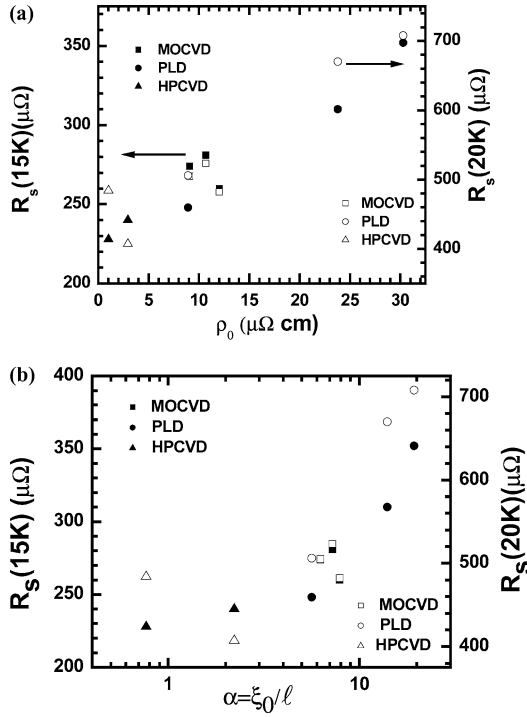
**Fig. 1.** The dependence of $R_s$ at 15 K (solid symbol) and 20 K (open symbol) on (a) $\rho_0$, normal-state resistivity right above $T_c$ (b) $\alpha = \xi_0/\lambda$, where $\xi_0$ is the BCS coherence length and $\lambda$ is the electronic mean free path.

conventional superconductor, the dependence of $R_s$ on the material properties could be described within BCS-theory by the material parameters $\lambda_L$, $v_F$, $\Delta(0)$ and $\lambda$ or the two dimensionless quantities $\alpha = \xi_0/\lambda$ and $\gamma(\lambda = \infty) = \lambda_L/\xi_0$. Here, $\xi_0$ is the BCS coherence length, $v_F$ is Fermi velocity, $\lambda_L$ is the London penetration depth, and $\lambda$ is the electronic mean free path. Because our study is restricted to MgB$_2$ samples only, $\gamma$ is a constant, and only the $R_s$ dependence on $\alpha$ can be addressed. Figure 1b shows the dependence of $R_s$ on the material parameters $\alpha = \xi_0/\lambda$ at 15 K (solid symbol) and 20 K (open symbol). $\alpha$ could be calculated from the extracted quantities $R_s(T)$, $\lambda(0)$, $\Delta_\pi(0)$ and $\rho_0$ from the temperature dependence of $Z_s$ [17,32,33]. Here we only consider the $\pi$-band coherence length. There is another coherence length corresponding to the $\sigma$ band. However, we have found in our previous work the conductivity is dominated by the $\pi$ band [33]. In Fig. 1b, the $R_s$ decrease on $\alpha$ in different rate. It decrease rapidly with $\alpha$, then slowly decrease when $\alpha$ is below around 2. According to BCS theory, $R_s$ is expected to decrease with decreasing $\alpha$ and saturates around $\alpha = 0.7$, but increases again as $\alpha$ decreases further [34]. Our ob-

servation is similar to the BCS calculation. However, so far, we could not find the expected saturation in our measurement because of our limited resolution for $R_s$. In addition, for the 100-nm thick epitaxial film on Al$_2$O$_3$ substrate there is a 30–40-nm thick non-superconducting layer between the Al$_2$O$_3$ substrate and MgB$_2$ thin film [31]. For the analysis of the surface impedance of this particular film we assumed the thickness of the superconducting layer to be 62 nm: For this value the best agreement between the dc resistivity determined from microwave and dc measurements was achieved.

We plot in Fig. 2 the temperature dependences of $R_s$ below 20 K for the samples with the lowest $R_s$ value for each type of orientation. It is found that temperature dependences are similar although the orientations are completely different. As we knew, the different orientations of the grains in the film will produce the grain boundaries between the grains. The RF current may be blocked by the boundaries yielding a percolation effect, or pass through the boundaries with boundary resistance $R_{bn}$. These two effects lead to additional RF losses. The sizes of percolation effect and $R_{bn}$ are usually dependent on the misorientation angle of the grains in the film. Consequently, the epitaxial films usually have a lower RF loss than the random orientation films. The above observation in Fig. 2 indicates the grain boundary may not have an important contribution to $R_s$ for low $\rho_0$ thin film. This explanation could be further verified as follows: Firstly, DC measurement could give an estimate on the contribution of grain boundaries. Figure 3 shows the temperature dependence of $\rho$ up to room temperature for a random orientation film.
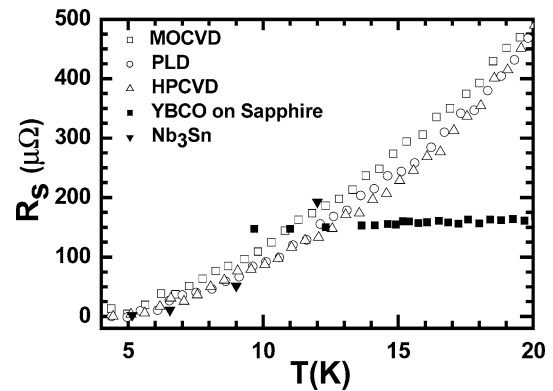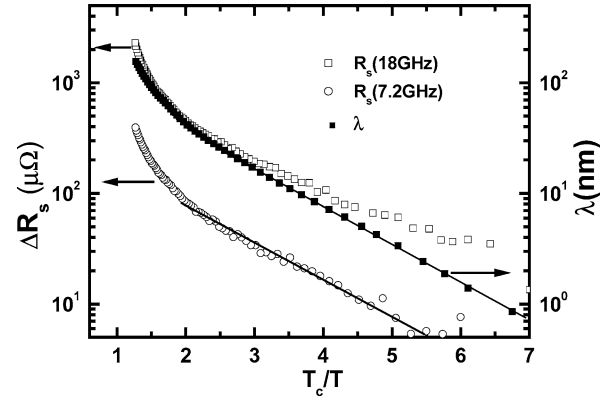


**Fig. 2.** Comparison of surface resistance of MgB$_2$ with YBCO, and Nb$_3$Sn films. The $R_s$ curves of MgB$_2$ thin films represent the best $R_s$ values for films of different crystalline orientations.
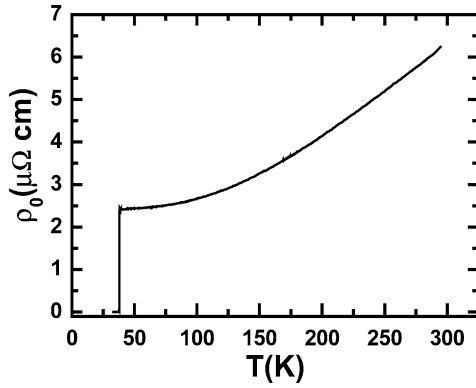
**Fig. 3.** Typical resistivity versus temperature for a random orientation film made by CVD method.



**Fig. 4.** Logarithmic representations of change of $R_s$ at 18 GHz (open square), 7.2 GHz (open circle) and penetration depth $\lambda$ (solid square) versus $T_c/T$ below 30 K. The linear behavior represents $\Delta R_s$ and $\lambda$ follow $\exp(-\Delta/kT_c)$. The solid line is depicted for the guide of clearance. Two solid lines have the same slope.

$\Delta\rho$ of about 3.5 $\mu\Omega$ cm could be found from this figure. The typical value of $\Delta\rho$ for *c*-axis orientation and epitaxial films could also be found in Refs. [30,31]. All the results show $\Delta\rho(\rho_{300K}-\rho_{50K})$ ranges from 3.5 to 7 $\mu\Omega$ cm for the above three kinds of samples. These values are similar to that from single-crystal measurement [36,37]. So, the grains in the films are well connected. The RF current flows in a straight path, and grain boundaries effect can be neglected. Secondly, the BCS coherence length is about 50 nm, the mean free path for these three samples is about 10 nm. This leads to an effective coherence length of about 10 nm. Hence, a strong coupling exists between two adjacent grains, and the current density almost remains the same when the current passes the grain boundary, which makes the grain boundary resistance very small. Thirdly, the temperature dependences follow $\exp(-\Delta_\pi(0)/kT)$ approximately, where $\Delta_\pi(0)$ is the energy gap of $\pi$-band. Figure 4 shows logarithmic plot of $R_s$ and penetration depth $\lambda$ versus $T_c/T$ at the temperature below 30 K. A good linear behavior could be found from penetration depth data. The solid line is depicted for the guide of clearance. However, $R_s$ values deviate from linear behavior at about 9 K. It is caused by the resolution of our measurement. As we have demonstrated in our previous paper, the rutile resonator could achieve a higher resolution on $R_s$ [17]. The change of $R_s$, $\Delta R_s$, from rutile resonator measurement is also depicted in Fig. 4. The better linear behavior down to 7 K is found. Here, the solid line, which lies on the data at 7.2 GHz, is of the same slope as the previous one. Hence, we believe the temperature dependences of $\Delta R_s$ should follow $\exp(-\Delta_\pi(0)/kT)$. It implies that grain boundary

effect do not play an important role in our measurement on low normal-state resistivity samples.

Low $R_{res}$ (<50 $\mu\Omega$ at around 18 GHz) is observed in our measurement, i.e., $R_{res}$ is less than around 20 $\mu\Omega$ at 10 GHz if $\omega^2$ scaling law is used. This value is much lower than that in the early reports, which gave values ranging from 300 $\mu\Omega$ to 4.7 m$\Omega$ [18–21]. However, recent report after the intensive efforts on the film deposition techniques, gave $R_{res}$ lower than 50 $\mu\Omega$ at 10 GHz, which is similar to our present data [17,22]. In addition, $R_s$ values of Nb$_3$Sn ($T_c = 18$ K) and high-quality epitaxial YBCO films deposited on r-cut sapphire are also depicted [8, 38]. We can easily see that MgB$_2$ has the lowest $R_s$ between 10 K and 1 4 K. From the cryogenic cooling point of view, 10 to 14 K can make a big difference from 4 K, in particular with regard to cost and power efficiency of closed-cycle refrigerators. Hence, MgB$_2$ thin films have demonstrated its advantage over other superconductors working around 10 K for microwave applications.

## 4. THZ MEASUREMENT

Using TDTS, we also measured the epitaxial MgB$_2$ film ($T_c = 39.1$ K) on Al$_2$O$_3$ mentioned above. Our setup utilizes ultrashort broadband THz pulses generated and detected, respectively, by optical rectification and electro-optic sampling in 1-mm thick [110]-oriented ZnTe single crystal [27,28]. This technique enables measuring the amplitude as
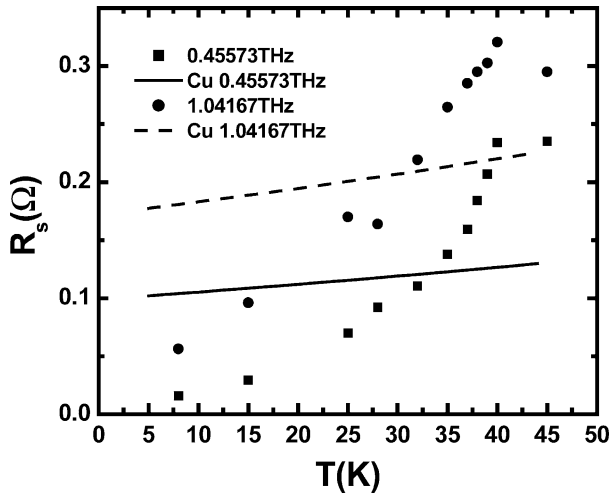
**Fig. 5.** Temperature dependence of $R_s$ at 0.445 and 1.0 THz. The $R_s$ of copper at the same frequency is also depicted for comparison.



**Fig. 6.** Frequency dependence of $R_s$ at THz. The solid line represents the values scaled from $R_s$ at 18 GHz following to $\omega^n$ with $n = 1.5$.

well as the phase shift of the transmitted THz wave; therefore the complex dielectric response(or, equivalently, the complex conductivity of the MgB$_2$ thin film) can be calculated without any model assumption and without Kramers–Kronig transformation. The experimental setup, the principle of the measurement, and the method of extraction of the complex are described in [27, 28].

Figure 5 shows the temperature dependence of the deduced $R_s$, the real part of $Z_s = (j\omega\mu/\sigma)^{0.5}$, at two frequencies, 0.455 and 1 THz. The temperature dependence of $R_s$ for copper is also depicted for comparison [39]. From this figure it is found that $R_s$ for MgB$_2$ is lower than that of copper below $T_c$ in the submillimeter wave and THz regions, in particular, $R_s$ of MgB$_2$ is about three times lower at 450 GHz around 15 K. Some measurements for YBCO showed that the $R_s$ value of 0.45 $\Omega$ at 1 THz and 15 K, which is about four times higher than MgB$_2$ [40, 41]. Hence, MgB$_2$ thin film has also shown its advantages in the THz region.

Figure 6 shows the frequency dependence of $R_s$ at 15 K (solid symbol). Usually, $R_s$ at frequency below the gap frequency follows $\omega^n$, where n is power index. We scaled $R_s$ measured with sapphire resonator at around 18 GHz to THz according to $\omega^n$ scaling law, yielding goods fit with $n = 1.5$. This does not agree with the report in microwave region, where $n = 2$ was found [19]. Therefore, this film is also measured with rutile resonator at 7.2 GHz. Figure 6 shows the temperature dependence of $R_s$ at
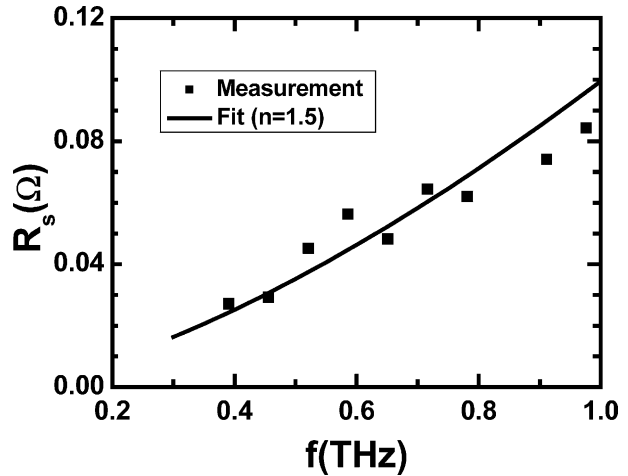
18 and 7.2 GHz below 25 K, respectively (Fig. 7). The inset shows the $R_s$ at 7.22 GHz is scaled to 18 GHz, yielding the best fit with $n = 1.9$. This $n$ value is approximately equal to the reported value in microwave measurement [19]. Also, it is approximately equal to that obtained for Nb measurement, which could be explained in the BCS model [42]. These measurements indicate that n decrease with the increase of frequency. MgB$_2$ thin film will benefit from this change for the electronic application in THz.
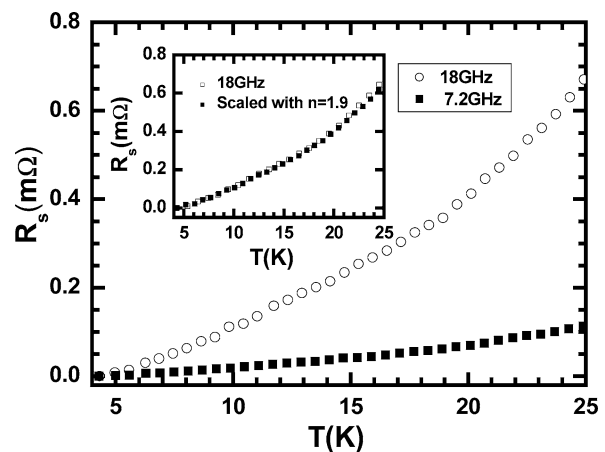


**Fig. 7.** The temperature dependence of $R_s$ at 18 and 7.2 GHz. The inset shows $R_s$ value at 18 GHz and scaled $R_s$ from 7.2 to 18 GHz following $\omega^n$ with $n = 1.9$.

## 5. DISCUSSIONS AND CONCLUSIONS

We have firstly illustrated in the above the $R_s$ at microwave. The low $R_s$ value below 50 $\mu\Omega$ at 18 GHz could be achieved by several kinds of deposition techniques. This is a great progress in making the film because very low $R_s$ could be repeatedly obtained. We also found that $R_s$ decrease almost linearly with $\rho_0$. This may provide a direction to optimize the deposition techniques to reduce further $R_s$ value. The comparison between $MgB_2$ thin film and $Nb_3Sn$ and YBCO indicates a temperature nicht (10–14 K), in which $MgB_2$ is of the lowest $R_s$. The temperature dependence of $R_s$ shows the intrinsic properties could be obtained. The recent calculations have presented a low intrinsic nonlinear effect in $MgB_2$ thin film compared with YBCO material [43]. These results are significant for superconducting planar circuit. This kind of circuit is compact and light with high performance [10]. However, the current density in the center strip of the circuits will peak at the edge of strip, which will produce large nonlinear effect for HTSC planar circuits, even at moderate power level due to weak link and flux penetration, although high intrinsic power handling is predicted [44–47]. In contrast to YBCO thin film, the intrinsic property of $MgB_2$ thin film could be much easier to achieve due to long coherence length as discussed in the above [43]. It means microwave devices made of $MgB_2$ thin film is of high power handling. Hence, $MgB_2$ offers the great promising for superconductive passive microwave devices [48].

The $R_s$ at THz indicates a lower value than YBCO and normal metal. This means contacts and passive structure in THz superconducting circuits, for example, antenna, could also be made from $MgB_2$ thin films, in contrast to the present THz devices, in which the contacts and passive structure is commonly made from normal metal [13]. In addition, $MgB_2$ may be suitable for fabricating Josephson junction because it has less anisotropy, fewer material complexities, and a longer coherence length [49]. There are some reports on investigating multilayers of $MgB_2$ thin films with several other materials, and making successful sandwich-type $NbN/AlN/MgB_2$ junction [50–52]. However, there is, so far, no successful report on fabricating $MgB_2$/insulator/$MgB_2$ junction, which is referred as all $MgB_2$ tunneling junction. One of the future challenges is the fabricating of all $MgB_2$ THz detector with all $MgB_2$ tunneling junctions to replace niobium tunneling junctions working above 20 K.

## 6. ACKNOWLEDGMENTS

## REFERENCES

1. J. Nagamatsu, N. Nakagawa, T. Muranaka, Y. Zenitani, and J. Akimitsu, *Nature* **410,** 63 (2001).
2. J. Kortus, I. I. Mazin, K. D. Belashchenko, V. P. Antropov, and L. L. Boyer, *Phys. Rev. Lett.* **86,** 4656 (2001).
3. H. J. Choi, D. Roundy, Hong Sun, M. L. Cohen, S. G. Louie, *Nature ,* 758 (2002).
4. I. I. Mazin, *et al.*, *Phys. Rev. Lett.* **89,** 107002 (2002).
5. T. Dahm and N. Schopohl, *Phys. Rev. Lett.* **91,** 017001 (2003).
6. P. Szabo, *et al.*, *Phys. Rev. Lett.* **87,** 137005 (2001).
7. H. Uchiyama, *et al.*, *Phys. Rev. Lett.* **88,** 157002 (2002).
8. M. A. Hein, *High-Temperature Superconductor Thin Films at Microwave Frequency, Vol. 155: Springer Tracts of Modern Physics* (Springer, Heidelberg, 1999).
9. T. Van Duzer, and C. W. Tunner, *Principle of Superconductive Devices and Circuits*, Prentice Hall, Englewood Cliffs, NJ.
10. N. Klein, *Rep. Prog. Phys.* **65,** 1387 (2002).
11. A. D. Semenov, G. N. Gol'tsman, and R. Sobolewski, *Supercond. Sci. Technol.* **15,** R1 (2002).
12. B. D. Jackson, T. M. Klapwijk, *Physica C* **372–376,** 368 (2002).
13. M. Hajenius, *et al.*, *Supercond. Sci. Technol.* **17,** S224 (2004).
14. M. A. Hein, M. Getta, S. Kteiskott, B. Mönter, H. Piel, D. E. Oates, P. J. Hirst, R. G. Humphreys, H. N. Lee, and S. H. Moon, *Physica C* **372–376,** 571 (2002).
15. M. R. Eskildsen et. al., *Phys. Rev. Lett.* **89,** 187003 (2002).
16. B. B. Jin et. al., *Supercond. Sci. Technol.* **18,** L1 (2005).
17. B. B. Jin, *et al.*, *Phys. Rev. B* **66,** 104521 (2002).
18. A. Andreone, *et al.*, *Physica C* **372–376,** 1287, (2002).
19. A. A. Zhukov, *et al.*, *Appl. Phys. Lett.* **80,** 2347 (2002).
20. A. J. Purnell, *et al.*, *Supercond. Sci. Technol.* **16,** 1 (2003).
21. A. Andreone, E. Di Gennaro, G. Lamura, F. Chiarella, and R. Vaglio, *J. Superconductivity* **16,** 807 (2003).
22. N. Hakim, C. Kusko, S. Sridhar, A. Soukiassian, X. H. Zeng, and X. X. Xi, *Appl. Phys. Lett.* **81,** 4525 (2002).
23. G. Lamura, A. J. Purnell, L. F. Cohen, A. Andreone, F. Chiarella, E. Di Gennaro, R. Vaglio, L. Hao, and J. Gallop, *Appl. Phys. Lett.* **82,** 4525 (2003).
24. R. A. Kaindl, M. A. Carnahan, J. Orenstein, D. S. Chemla, H. M. Christen, H. Y. Zhai, M. Paranthaman, and D. H. Lowndes, *Phys. Rev. Lett.* **88,** 027003 (2002).
25. A. V. Pronin, A. Pimenov, A. Loidl, and S. I. Krasnosvobodtsev, *Phys. Rev. Lett.* **87,** 097003 (2001).

26. J. H. Jung, *et al.*, *Phys. Rev. B* **65,** 052413 (2002).
27. M. Kempa, P. Kuzel, S. Kamba, P. Samoukhina, J. Petzelt, A. Grag, and Z. H. Barber, *J. Phys.: Cond. Matter* **15,** 8095 (2003).
28. J. Petzelt, P. Kuzel, I. Rychetsky, A. Pashkin, and T. Ostrapchuk, *Ferroelectrics* **288,** 169 (2003).
29. S. F. Wang, *et al.*, *Thin Solid Film* **443,** 120 (2003).
30. W. N. Kang, H.-J. Kim, E.-M. Choi, C. U. Jung, S.-I. Lee, *Science* **292,** 1521–1523 (2001).
31. X. H. Zeng, *et al.*, *Nature Mater.* **1,** 35–38 (2002).
32. N. Klein, N. Tellmann, H. Schulz, K. Urban, S. A. Wolf, and V. Z. Kresin, *Phys. Rev. Lett.* **71,** 3355 (1993).
33. B. B. Jin, *et al.*, *Phys. Rev. Lett.* **91,** 127006 (2003).
34. J. Halbritter, *Z. Physik* **243,** 201 (1971); *Z. Physik* **266,** 209 (1974).
35. J. Halbritter, *Supercond. Sci. Technol.* **14,** R17 (2003).
36. J. M. Rowell, *Supercond. Sci. Technol.* **16,** R17 (2003).
37. Hyeong-Jin Kim, W. N. Kang, Eun-Mi Choi, Mun-Seog Kim, Kijoon H. P. Kim, and Sung-Ik Lee, *Phys. Rev. Lett.* **87,** 087002 (2001).
38. J. Einfeld, P. Lahl, R. Kutzner, R. Wördenweber, G. Kästner, *Physica C* **103,** (**2001**).
39. A. N. Luiten, M. E. Tobar, J. Krupka, R. Woode, E. N. Ivanov, and A. G. Mann, *J. Phys.D: Appl. Phys.* **31,** 1383 (1998).
40. I. Wilke, M. Khazan, C. T. Rieck, P. Kuzel, T. Kaiser, C. Jaekel, and H. Kurz, *J. Appl. Phys.* **87,** 2984 (**2000**).
41. I. Wilke, M. Khazan, C. T. Rieck, P. Kuzel, C. Jaekel, and H. Kurz, *Physica C* **341-348,** 2271 (2000).
42. J. P. Tuneaure, J. Halbritter, and H. A. Schwettman, *J. Supercond.* **4,** 341 (1991).
43. T. Dahm, and D. J. Scalapino, *Appl. Phys. Lett.* **85,** 4436 (2004).
44. P. Lahl and R. Wördenweber, *Appl. Phys. Lett.* **81,** 505 (2002).
45. P. Lahl and R. Wördenweber, *Supercond. Sci. Technol.* **17,** S369 (2004).
46. J. Halbritter, *J. Supercond.* **8,** 691 (1995).
47. T. Dahm, and D. J. Scalapino, *Appl. Phys. Lett.* **69,** 4248 (1996).
48. N. Klein, *et al.*, *IEEE Trans. Appl. Supercond.* **13,** 3252 (2003).
49. M. Naito, and K. Ueda, *Supercond. Sci. Technol.* **17,** R1 (2004).
50. X. X. Xi, *et al.*, *Supercond. Sci. Technol.* **17,** S196 (2004).
51. H. Ake, *J. Appl. Phys.* **96,** 2343 (2004).
52. H. Shimakage, K. Tsujimoto, Z. Wang, and M. Tonouchi, *Supercond. Sci. Technol.* **17,** 1376 (2004).